Strained germanium nanowire optoelectronic devices for photonic-integrated circuits

Qi, Zhipeng; Sun, Hao; Luo, Manlin; Jung, Yongduck; Nam, Donguk

2018

Qi, Z., Sun, H., Luo, M., Jung, Y., & Nam, D. (2018). Strained germanium nanowire optoelectronic devices for photonic-integrated circuits. Journal of Physics: Condensed Matter, 30(33), 334004-. doi:10.1088/1361-648x/aad0c0

https://hdl.handle.net/10356/136706

https://doi.org/10.1088/1361-648X/aad0c0

Strained germanium nanowire optoelectronic devices for photonic-integrated circuits

Zhipeng Qi[1], Hao Sun[1], Manlin Luo[1], Yongduck Jung[1], and Donguk Nam[1,*]

[1]School of Electrical and Electronic Engineering, Nanyang Technological University, 50 Nanyang Avenue, 639798 Singapore, Singapore.

*E-mail: dnam@ntu.edu.sg

Keywords: Nanowire, germanium, strain, optoelectronics, photonic-integrated circuits

Abstract: Strained germanium nanowires have recently become an important material of choice for silicon-compatible optoelectronic devices. While the indirect bandgap nature of germanium had long been problematic both in light absorption and emission, recent successful demonstrations of bandstructure engineering by elastic strain have opened up the possibility of achieving direct bandgap in germanium, paving the way towards the realization of various high-performance optical devices integrated on a silicon platform. In particular, the latest demonstration of a low-threshold optically pumped laser in a highly strained germanium nanowire is expected to vitalize the field of silicon photonics further. Here, we review recent advances and challenges in strained germanium nanowires for optoelectronic applications such as photodetectors and lasers. We firstly introduce the theoretical foundation behind strained germanium nanowire optoelectronics. And several practical approaches that have been proposed to apply tensile strain in germanium nanowires are further discussed. Then we address the latest progress in the developments of strained germanium nanowire optoelectronic devices. Finally, we discuss the implications of these experimental achievements and the future outlook in this promising research field.

1. Introduction

In recent years, germanium (Ge) has shown great potential for photonic-integrated circuits (PICs) owing to its superior optical properties over silicon (Si) [1]. While Si is a distinct indirect bandgap material with a very large energy difference of 2.4 eV between the direct and indirect bandgaps [2], Ge is a pseudo-direct bandgap semiconductor due to its small energy difference of 136 meV between the direct Γ- and indirect L-valley minimum points [3,4]. This pseudo-direct nature of Ge allows direct bandgap absorption and recombination near the band edge, whereas inefficient indirect bandgap transition is dominant in Si. Therefore, various optoelectronic devices using Ge such as photodetectors [5–27] and modulators [28–34] have been demonstrated during the past few decades.

However, the realization of fully functional PICs adopting these Ge-based optical devices as building blocks still faces formidable challenges because of the physical limitations imposed by Ge's bandstructure. Although the absorption coefficient for bulk Ge within the wavelength of 1300 ~ 1475 nm is comparable to group III-V compounds such as InGaAs, GaN, etc., it drops dramatically at the wavelength exceeding 1500 nm and becomes nearly one-twentieth compared to those for III-V materials at 1550 nm which is a technologically important telecom wavelength for optical interconnects [6,35–37]. Therefore, much thicker Ge layers are usually needed for the use of light detection to achieve large enough absorption in the near-infrared region (NIR) at the cost of a slower operation speed.

The problem is even more evident for Ge-based light emitters. Although Ge's pseudo-direct bandgap allows some conduction electrons to populate the direct Γ-valley and recombine with

holes in a radiative way, the fraction of such electrons occupying the direct Γ-valley is extremely low (<0.01%) [38] because of a much smaller density of states for the Γ-valley compared to the slightly lower indirect L-valley [39]. This causes a very low light emitting efficiency (<1%) [38]. Nevertheless, desired population inversion and optical gain have been theoretically demonstrated in Ge utilizing a combination of heavy n-type doping (>1×10^{19} /cm^3) and residual biaxial tensile strain (~0.2%) [1]. Here, the residual strain lowers the energy difference between the two conduction valleys, while the n-type doping increases the fraction of electrons in the Γ-valley by filling up the L-valley, thereby enhancing the feasibility of population inversion. Based on this concept, researchers successfully demonstrated both optically and electrically pumped Ge lasers [40–42].

These experimental demonstrations have made a big step towards the realization of PICs, but there was still plenty of room for the further dramatic improvements of such technologies. For example, the lasing threshold was too high (~280 kA/cm^2) to be used in power-efficient PICs possibly owing to the yet unfavorable Ge's indirect bandgap. Therefore, it was considered crucial to engineer Ge's bandstructure to reduce the energy difference, and if possible, even invert the two conduction valleys to achieve direct bandgap in Ge [43,44]. Among various approaches including tin (Sn) alloying [45], strain engineering has shown a great promise for modifying bandstructure and enhancing both radiative recombination and optical gain of Ge [44,46].

In 2009, a couple of theoretical modeling showed that dramatic enhancements in optical properties of single-crystal Ge could be achieved by applying large mechanical tensile strain of a few percent [43,44]. Such a large strain value, however, is difficult to realize in bulk Ge experimentally.

Typically, the ideal strength for a perfect crystalline Ge is estimated to be in the range of 14 ~ 20 GPa, while a bulk Ge shows a much smaller fracture strength of 40 ~ 95 MPa [47,48], which tends to fracture easily with a strain in the order of a fraction of 1%. In comparison to bulk materials, nanowire (NW) structures exhibit much higher fracture strengths and smaller density of defects owing to their large surface area to volume ratios and self-purification [49–52]. As reported by T. Zhu and J. Li [53], NWs can be several tens of times stronger per area than its bulk form, validating the fact that 'smaller is stronger'. This property makes Ge NWs an ideal platform for applying large mechanical strain for bandstructure engineering. For example, a high tensile strain of ~17% that approaches the ideal fracture strength of Ge has already been demonstrated in Ge NWs without any mechanical fractures [54]. This strain value is nearly two orders of magnitude higher than the observed one in bulk Ge [55], and also far beyond the calculated value for the indirect-to-direct bandgap transition [43,56]. This experimental demonstration has made strained Ge NWs a promising material platform for Si-compatible optoelectronic devices that can be used in PICs.

In this paper, we will make an overview of recent developments of strained Ge NWs for optoelectronic applications. Although there have been some reviews putting the focus on the aspects of bandstructure engineering in Ge [57] or Ge-based optical devices [4,58], we will mainly review the studies on strained Ge NW optoelectronic devices. The organization of this paper is as follows. Section 2 introduces the theoretical background of strain engineering in Ge and discusses the effects of strain on Ge's optical properties. Section 3 describes various methods as to how to apply tensile strain in Ge NWs effectively. Section 4 presents latest applications of strained Ge NWs for optoelectronic devices and their performances. Section 5 provides conclusions and also discusses possible challenges for Ge NW optoelectronics.

2. Theory on strained Ge

In semiconductor materials, radiative recombination is mainly dominated by direct bandgap optical transition, for which the same momentum is required for the electrons in the conduction bands (CBs) and the holes in the valence bands (VBs) [57]. For indirect bandgap optical transition, electron-hole recombination occurs with the assistance of phonon, releasing energy as heat rather than photon. Since Ge's pseudo-direct bandgap nature makes the indirect bandgap optical transition dominant over the direct bandgap optical transition, light emission in Ge had long been regarded as a challenging task.

As shown in Fig. 1(a), the bandstructure of bulk Ge shows a minimum point of the CB at the L-valley in the 1st Brillouin zone (BZ), which is about 136 meV below the Γ-valley minimum point [4]. According to the Fermi-Dirac (F-D) statistic distribution and also because of a much larger density of states in the L-valley, most of the injected electrons will preferentially occupy the L-valley [59]. Although the higher direct Γ-valley can also be populated with some injected electrons via heavy n-type doping suggested by the researchers at MIT, the fraction of electrons in the Γ-valley is still quite small (<0.01%) under this situation [60]. Therefore, the light emitting efficiency of Ge in its natural form is greatly limited.

To improve the light emitting efficiency of Ge, mechanical strain engineering was proposed since large tensile strain can significantly modify Ge's bandstructure [43,44]. Figure 1(b) shows that the Γ-valley of strained Ge can become lower than the L-valley with a sufficient amount of strain, thus increasing the fraction of electrons in the Γ-valley. In addition, strain also leads to the splitting of

two degenerated VBs (*i.e.*, the heavy- and the light-hole bands). The splitting of these two VBs will contribute to the reduction of the required amount of injected holes for achieving population inversion, which can further lower the lasing threshold [1,61,62].

Based on deformation potential theory [56], changes of Ge's bandgap energies for uniaxial and biaxial tensile strain can be calculated as shown in Figs. 1(c) and (d) [63]. Because the heavy- and light-hole VBs are degenerate in the absence of strain, only two bandgap energies exist in unstrained Ge, that is, Γ-valley to VB at 0.8 eV and L-valley to VB at 0.664 eV. Once uniaxial or biaxial tensile strain is introduced to Ge, 4 possible bandgap energies emerge: Γ-valley to heavy-hole band (Γ-HH), L-valley to heavy-hole band (L-HH), Γ-valley to light-hole band (Γ-LH), and L-valley to light-hole band (L-LH). As shown in Figs. 1(c) and (d), the bandgap energy of Γ-HH (Γ-LH) reduces faster than the one of L-HH (L-LH), indicating that the energy difference between Γ- and L-valleys becomes smaller at higher tensile strain. The theoretical calculations also demonstrate that Ge can be transformed into a direct bandgap material at a uniaxial (biaxial) tensile strain exceeding the crossover point of ~ 4.6% (~1.7%).

F. Zhang *et al*. theoretically studied the effect of uniaxial tensile strain along the <111> direction in Ge NWs, and suggested an effective way to achieve a direct bandgap Ge based on first-principles calculations [43]. In Fig. 2(a), $E_{\Gamma-L}$ denotes the energy difference between the Γ- and L-valleys, M_{vc}^{l} refers to longitudinal optical transition matrix element, and ϵ_l is the longitudinal strain along the <111> direction. M_{vc}^{l} has a sudden jump to a nonzero value for ϵ_l > 3.5% due to the drop of the Γ-valley in energy with respect to the L-valley, indicating that the direct bandgap transition is significantly enhanced. A rapid downshift of $E_{\Gamma-L}$ could even induce an indirect-to-

direct transition with a larger ϵ_l of 5.3%, making Ge the material of choice for lasing applications. With the direct bandgap narrowing, a substantial redshift of absorption spectrum could also be expected along with the increase of absorption at the technologically important telecom wavelength (~1550 nm).

D. Sukhdeo *et al.* also performed theoretical calculations on how much light emitting efficiency of Ge can be improved as a function of uniaxial tensile strain along the <100> direction [38]. Figure 2(b) shows the calculated results of internal quantum efficiency (IQE) at different strain values for various non-radiative recombination lifetimes. The IQE of Ge can be improved greatly with a longer defect-limited minority carrier lifetime which corresponds to a smaller non-radiative recombination rate [64,65]. On the other hand, the strain-induced increase of electron population in the Γ-valley results in a larger radiative recombination rate, and therefore, IQE also increases with strain.

Furthermore, B. Dutt *et al*. provided a theoretical analysis of the relative merits of biaxial tensile strain as well as n-type doping as approaches to achieve a power-efficient Ge laser [60,66]. In their quantitative analysis with tight-binding modeling, the threshold current density of a double-heterostructure Si/Ge/Si laser is calculated as a function of strain value and doping level, as shown in Fig. 2(c). It is found that the biaxial tensile strain lowers the lasing threshold significantly at a certain doping concentration, showing a much stronger impact on Ge lasers compared to the doping level. It should also be noted that the effect of n-type doping is not always positive especially for the case of a larger tensile strain. For instance, the lasing threshold starts increasing with a doping level of $>5 \times 10^{19}$ /cm^3 when Ge is under ~1.5% biaxial tensile strain, highlighting

the importance of a careful optimization of both strain and doping for the ultimate reduction of Ge's lasing threshold. Theoretically, the optimal n-type doping level that leads to the lowest threshold current density decreases from 1.5×10^{20} to 1×10^{18} /cm^3 with the increase of tensile strain from 0 to 4%.

To study the strain-related properties of Ge NWs, A. Lee *et al*. have made theoretical estimations on mechanical and electronic properties for <100>, <110>, and <111> strained Ge NWs by using density-functional theory [67]. As illustrated in Fig. 2(d), Young's modulus is given as a function of Ge NW diameters with different growth directions, which is calculated based on the second-order derivative of energy to strain. The size-dependent behavior of Young's modulus is similar for the <100> and <111> NWs, both of which show the same tendency with the decrease of the NW diameter. However, the Young's modulus in the <110> Ge NW is observed less sensitive to the diameter, and this could be explained by the surface effects; the <100> and <111> NWs share equivalent surface facets whereas the <110> NW contains different ones. The Young's moduli of NWs in all three directions end up being slightly higher than their bulk values, which may be induced by different surface geometries and bonding effects. This work provides quantitative information about the effects of the growth direction and the strain of Ge NWs on mechanical properties and bandstructures, which should be very useful in designing and fabricating practical Ge NW optoelectronic devices.

3. Approaches to apply tensile strain in Ge nanowires

Strain engineering has been demonstrated to be a powerful tool to improve the performance of electronic/photonic devices [16,68–70]. For example, upon the application of a large mechanical

tensile strain to Ge NWs, the locations of band edges in Ge's bandstructure can be dramatically shifted, possibly transforming Ge into a direct bandgap material (Figs. 1(c) and (d)). Several innovative approaches have thus far been proposed to apply tensile strain in Ge NWs including mechanical bending, deposition of stressors, epitaxial growth, and microelectromechanical systems (MEMS) technique [54,71–77].

D. Smith *et al.* successfully induced a large mechanical strain in a Ge NW by mechanically bending it with two tungsten probes as shown in Fig. 3(a) [54]. Figures 3(b)-(d) show high-resolution transmission electron microscope (TEM) images of a bent Ge NW. In addition to the crack formation, a sudden and well-defined phase transformation from single crystal to amorphous structure was observed at the maximum strain position of the bent NW. This amorphization can be attributed to a gradual increase of disorder formed by crystal dislocations which take place prior to the fracture [78]. Figure 3(e) presents the maximum bending radius of curvature for Ge NWs with different diameters. The applied strain was determined by its bending degree which could be derived and calculated on the basis of the radius of curvature (Fig. 3(f)). The maximum applied strain increased from 4% to 17% as the diameter of Ge NWs was decreased. An extremely high bending strength up to ~18 GPa in the NW was demonstrated with a small diameter (20 ~ 25 nm). This report presents the merits of Ge NWs compared to its bulk counterpart for inducing a large enough mechanical tensile strain to dramatically improve the performance of Ge-based optoelectronic devices.

A more practical approach to introduce tensile strain in Ge is to employ external stressor layers [70,71,79–86]. There have been several works adopting this method to fabricate highly strained

Ge nanostructures such as the sputtering of a tungsten stressor on the backside of a Ge membrane [83,84] and the deposition of patterned Si_3N_4 films on a Ge layer [85,86]. Fig. 4(a) depicts that the tensile strained Ge NW can be realized through depositing a Si_3N_4 stressor layer on a pre-fabricated Ge NW waveguide [71]. It is observed that the strain could be transferred from the Si_3N_4 layer into the Ge NW. Furthermore, a modal optical gain of 80 cm^{-1} was successfully measured in a 0.6%-strained Ge NW by using variable stripe length method, indicating the significance of tensile strain in achieving an optical gain in Ge.

While the maximum tensile strain achieved by the approach in Ref. [71] is ~0.6%, M. Keplinger *et al.* demonstrated tensile strain higher than 1% in Ge NWs by using MEMS-based technique [72]. Figure 4(b) shows that a Ge NW connects a Si mesa pad on the left and a free-standing pre-strained cantilever which was initially pushed to the left by an oxidized mesa pad on the right. A substantial amount of strain could be introduced to the Ge NW by releasing the pre-stressed cantilever to induce a large position shift, which, in turn, stretches the Ge NW significantly. A variable strain value can be achieved by changing the position of Ge NWs and/or the stiffness of cantilevers. By using Raman spectroscopy and x-ray diffraction (XRD) measurement, a dominant tensile strain up to ~1.16% was observed in such Ge NWs.

As theoretically predicted by F. Zhang *et al.* [43], direct bandgap could be realized in Ge NWs grown along the <111> direction by inducing tensile strain. Such tensile-strained <111> Ge NW can be obtained by using core-shell structures [73]. Figure 4(c) shows a vapor liquid solid (VLS)-grown <111> Ge NW that is surrounded by a stressed amorphous SiN_x shell. The measured XRD

data reveals the presence of tensile strain up to 0.3% along the radius of the Ge core. The level of strain can be adjusted by changing the ratio of the SiN_x shell thickness to the Ge NW diameter.

Also, growing Ge NWs within the pores of mesoporous matrices offers a novel method to manipulate the structural configuration of NW arrays and adjust their aspect ratios as well as optical properties [73,74]. As shown in Fig. 5(a), high-quality Ge/SiO_2 nanocomposites could be prepared using supercritical fluid (SCF) method [74]. It is observed that the powder XRD (PXRD) peak position of the sample shifts to lower diffraction angle (2θ) values with the decrease of Ge NW diameter, resulting from the increased strain in the crystalline structure of NW induced by lattice expansion. More recently, self-assembled single-crystal Ge NWs embedded in InAlAs matrix was also demonstrated (Fig. 5(b)) [75]. The Raman peak of Ge/InAlAs nanocomposites is located at 284.5 cm^{-1} which is shifted from the one of bulk Ge at 301.3 cm^{-1}, revealing a ~3.8% tensile strain in the Ge NWs. The maximum tensile strain could reach 5.3% by changing the lattice constant of the matrix.

While highly tensile strained Ge NWs have been successfully prepared by above-mentioned methods, there still exist fundamental limitations for the practical use of those methods; those NWs are either not permanently strained or require special stressor architectures that are rather cumbersome during the fabrication process. Moreover, some of the preceding methods are not fully compatible with the mature CMOS fabrication process. Therefore, there was an urgent need to find a creative way to achieve permanent tensile strain in Ge NWs without adopting mechanical bending or any stressor layers which may also render the process incompatible with CMOS technology.

In 2012, R. Minamisawa *et al*. presented a novel structure that could induce a permanent, large mechanical tensile strain in Si NWs without any stressor layer [87]. As shown in Fig. 6(a), once the bridge NW is released from the substrate by under-etching, the two connection pads shrink in size as their residual tensile strains are relaxed, thereby pulling the central NW along its longitudinal direction. The uniaxial tensile strain in this NW can be flexibly adjusted by changing the device geometry (*e.g*., dimensions of NW and pads). Since this method only requires a simple and conventional lithography for straining NWs, it enables the creation of a large number of NWs with different amounts of tensile strain through a single-step lithography process. Due to its unique advantages, this technique has also been utilized for inducing permanent tensile strain in chip-integrated Ge NWs.

In 2013, two independent groups reported tensile strained Ge NW structures using the technique devised by R. Minamisawa *et al*., as shown in Figs. 6(b) and (c) [76,77]. Both experiments employed a Ge layer under a residual biaxial tensile strain, which is created owing to a large thermal expansion mismatch between Si and Ge during epitaxial growth [88]. Figure 6(b) shows the fabrication process flow [76]. A thin layer of chromium (Cr) was first deposited onto the starting Ge/Si-on-insulator (SOI) substrate as a hard mask, and then polymethyl methacrylate (PMMA) resist was coated onto Cr layer. After EBL patterning and dry etching, the underlying oxide layer was removed by wet etching, and as a result, the central Ge bridge is uniaxially strained due to the same mechanism used for strained Si NWs shown in Fig. 6(a). By simply varying the geometrical factors such as NW width or length, tensile strain can be fully customized. Since the

strain is created purely by elastic deformation, the maximum achievable strain is mainly determined by the ultimate strength of Ge that is as high as 15 GPa [49].

Meanwhile, this method is also promising for the introduction of double heterostructure effect within a homogeneous Ge NW. Conventional heterostructures are usually fabricated by stacking multiple layers of different materials, where a narrow bandgap material is sandwiched between two wide bandgap materials. However, the costly and complicated heteroepitaxy process is a huge obstacle for the realization of heterostructures. The technique presented by D. Nam *et al*. [77] avoids such problems of conventional methods but achieves the same heterostructure effect only by modulating spatial strain in Ge NWs. Figure 6(c) shows two types of strain-induced heterostructures; one is a strain-induced double heterostructure (s-DH) and another is a strain-induced graded double heterostructure (s-GDH). The corresponding spatial PL maps show that the light emissions can be highly concentrated in active regions (*i.e*., the created potential wells) arising from the spatially varying strain distributions. Although the size of the active region in Fig. 6(c) is in a micrometer scale that is much larger than the value for a typical double-heterostructure, it is highly feasible to scale down this active region by simply inducing the tensile strain in a much smaller spatial area. This approach provides a novel route to confine charge carriers at room temperature by tailoring the spatial strain profiles within Ge NWs, offering the possibility of realizing heterostructure lasers by a simple CMOS-compatible strain engineering process rather than complicated epitaxy techniques.

4. Optoelectronic devices based on strained Ge nanowires

As discussed in the preceding sections, a large mechanical tensile strain applied in Ge NWs has the ability to improve Ge's optical gain and, as a result, lower the threshold density for lasing. In addition, strained Ge NWs also possess excellent properties such as single-crystal nature, large refractive index, smooth surface, defect-free structure, and high absorption coefficient, which can be helpful to develop high-performance optoelectronic devices on a Si-compatible platform.

In addition to the arrayed Ge NW structures [5,74,89–91], an individual Ge NW that is strained by nanoelectromechanical (NEM) method has also shown a great promise for achieving high-performance, ultra-compact optoelectronic devices [11,16,92,93]. J. Greil *et al*. proposed a 3-point straining module with an individual Ge NW in the <111> direction which bridges between two isolated Si pads on an SOI substrate (Fig. 7(a)) [16]. In this structure, 3-point bending could induce a uniaxial tensile strain in Ge NWs. As the tensile strain in Ge NW is increased from 0 to 2.5%, Raman peak position shifts from ~300.5 cm^{-1} to a lower wavenumber of ~290 cm^{-1}. While the shape of the current-voltage (I-V) curve is found similar for all strain levels, the absolute current level increases over 1 order of magnitude with a 1.8% tensile strain, indicating that the conductivity of Ge NWs is enhanced by strain. Moreover, the increase of strain to 1.8% could induce a redshift of ~88 meV in the photocurrent spectra. The external quantum efficiency (EQE) of strained Ge NW is much higher than that of unstrained one in the NIR, especially within the wavelength range of 1550 ~ 1800 nm.

K. Guilloy *et al*. also reported similar results, where a Ge NW is strained up to 1.48% along the <111> direction by employing a patterned Si_3N_4 thin film (Fig. 7(b)) [11]. A p-i-n type Ge NW photodetector was anchored between two Si_3N_4 arms that induce mechanical tensile strain in the

Ge NW. The I-V curve of this strained Ge NW photodetector displays a very strong rectifying behavior, showing a nearly 5 orders of magnitude current change between forward and reverse bias voltages of 1 V. Since the tensile strain in the suspended Ge NW is greatly influenced by the length of pulling arms, it is possible to tune the amount of tensile strain flexibly by fabricating different arm lengths (L_{arm}). The photocurrent spectra of the Ge NW photodetectors exhibit an obvious redshift of the absorption cut-off from 0.8 to 0.73 eV as the strain is increased from 0 (L_{arm} = 0) to 1.48% (L_{arm} = 15 μm). Therefore, a tunable and wide detection range of 1200 ~ 1700 nm can be achieved in this configuration through selecting proper structural parameters (*e.g.*, L_{arm}). These findings and observations are of great importance for the design and fabrication of high-performance Ge-based photodetection devices. Since strain engineering can be performed in defect-free, single-crystal NWs, the proposed photodetectors based on Ge NWs can be an ideal platform for optoelectronic applications in PICs.

The last missing piece for fully functional PICs is chip-integrated lasers. Although III-V compound semiconductors such as gallium arsenide (GaAs) have been widely used for fabricating high-performance lasers, they are incompatible with Si-based fabrication process, thus inhibiting the integration of these lasers into CMOS architectures [57]. Therefore, the realization of Si-compatible lasers has long been regarded as the key to complete the toolbox for PICs.

The small energy difference between the Γ- and L-valleys in Ge has made a significant contribution to the development of Ge-based light sources. Over the past few years, researchers have experimentally demonstrated optical net gain and optically- and electrically-pumped lasing from Ge waveguide structures with a high n-type doping concentration [40–42]. Unfortunately,

the observed thresholds were too high possibly owing to the unfavorable bandstructure of n-type Ge, rendering the reports rather impractical although their scientific implications were substantial. As discussed in Section 2, the use of mechanical tensile strain is considered as one of the most promising solutions for making Ge, particularly Ge NWs, more favorable for laser applications.

By leveraging the strained NW platform introduced in Figs. 6(b) and (c), Bao *et al*. have recently demonstrated optically pumped lasing at a threshold density of 3 kW/cm^2, which is orders of magnitude smaller than the previous reports [92]. The Ge laser consists of a central Ge NW and a couple of distributed Bragg reflectors (DBRs) on stressing pads on both sides of the NW, as shown in Fig. 8(a). The DBRs allow achieving a high quality (Q) factor above 1000, and this device geometry enables a variable strain by changing the length of stressing pads [93]. In Fig. 8(b), a highly uniform tensile strain distribution was observed over the flat Ge NW with a large optical mode confinement factor of ~0.45. The simulations confirmed that this Ge NW could support a fundamental transverse electric (TE) mode at the peak emission wavelength of 1530 nm (Fig. 8(c)). With the pump power increased from 0.7 to 3.5 kW/cm^2, the PL spectra show a gradual transition from a broad spontaneous emission to lasing oscillation with a superlinear increase of intensity and a linewidth narrowing (Fig. 8(d)). It should be noted that the operating temperature was kept at 83 K. At the highest pump power, only the cavity modes around 1530 nm are permitted to enter into the lasing regime with optical net gain while other modes show saturation in intensity. These characteristics provide strong evidence of low threshold lasing in strained Ge NWs. This Ge NW laser significantly narrows the performance gap between Si-compatible lasers and III-V counterparts, making a big step closer to the realization of fully functional PICs.

5. Conclusions & Challenges

In conclusions, we have reviewed recent research progress in strained Ge NWs for optoelectronics. We have discussed the fundamental aspects of strained Ge and possible effects of strain on Ge-based optical devices. Herein, we have concluded that applying tensile strain in Ge NWs indeed shows a great promise for on-chip light sources and photodetectors since the tensile strain can modify the bandstructure of Ge towards the direct bandgap effectively, leading to the enhancement of both light emission and absorption at desired telecom wavelengths. We have also presented recent experimental efforts by various researchers to apply tensile strain in Ge NWs. Finally, active optoelectronic devices (*e.g.*, photodetectors) using strained Ge NWs have been introduced. We have also discussed the recent Ge NW laser that reports orders of magnitude lower lasing thresholds compared to the-state-of-the-art Ge-based lasers.

There still exist challenges in strained Ge NW optoelectronics, in particular, for lasing applications. Despite the promise provided by the recent result on Ge NW lasers [92], it is pivotal to obtain lasing at a high enough operating temperature such as 200 K and above to be employed with a commercially available thermo-electric cooler (TEC) while the paramount objective should be on the achievement of room temperature lasing. Recently, Gupta *et al.* have made a theoretical prediction that Ge can obtain a substantial optical net gain at room temperature with a uniaxial tensile strain of >4% [94]. Since this level of strain is already achieved experimentally in >200 nm thick Ge NWs in which a fundamental TE optical mode can be supported properly [38], such highly strained Ge NWs could be an ideal platform for the realization of room-temperature Ge NW lasers for PICs. The novel tunnelling injection to the direct Γ valley of highly strained Ge could also help lower the lasing threshold significantly [95].

It is also equally important to achieve electrically-driven lasers with strained Ge NW gain media. Lateral p-i-n diodes formed by ion implantation have been a natural fit for thin film-based light emitting devices, enabling efficient electrical injection into the active region for 1D and 2D electrically-pumped photonic crystal lasers [96,97]. Since ion implantation into Ge has been widely used to deliver a doping level of $>1 \times 10^{19}$ /cm^3 during the past decade [98,99], this lateral p-i-n diode approach can easily be extended to the strained Ge NW structures. By constructing a strain-induced heterojunction laterally and scaling down the active region to several tens of nanometers, the electrical delivery of excited carriers into the quantum-confined NW gain medium can be achieved.

Although great efforts have been spared in these aspects, there is still a long way to go for realizing practical electrically-pumped Ge lasers operating at room temperature. Hence, it is essential to investigate the fundamental properties and fabrication process of strained Ge NWs at the present stage. Moreover, the integration of strained Ge NW optoelectronic devices into Si-compatible PICs is also a great challenge for widespread applications of these lasers and photodetectors. In summary, the research field of strained Ge NWs is very promising for Si-compatible optoelectronics, and much more effort is still required to bring this research to fruition.

Acknowledgement

This work was supported by MOE under AcRF Tier 1 (RG 179/17) and Start-Up Grant (M4082093.040) from Nanyang Technological University (NTU) in Singapore. This work is also

supported by National Research Foundation of Singapore through the Competitive Research Program (NRF2017NRF-CRP001-003).

References:

[1] Liu J, Sun X, Pan D, Wang X, Kimerling L C, Koch T L and Michel J 2007 Tensile-strained, n-type Ge as a gain medium for monolithic laser integration on Si *Opt. Express* **15** 11272–7

[2] Xiang H J, Huang B, Kan E, Wei S H and Gong X G 2013 Towards direct-gap silicon phases by the inverse band structure design approach *Phys. Rev. Lett.* **110** 13–6

[3] Liu Z, Li Y, He C, Li C, Xue C, Zuo Y, Cheng B and Wang Q 2014 Direct-bandgap electroluminescence from a horizontal Ge p-i-n ridge waveguide on Si(001) substrate *Appl. Phys. Lett.* **104** 191111

[4] Liu J, Camacho-Aguilera R, Bessette J T, Sun X, Wang X, Cai Y, Kimerling L C and Michel J 2012 Ge-on-Si optoelectronics *Thin Solid Films* **520** 3354–60

[5] Polyakov B, Daly B, Prikulis J, Lisauskas V, Vengalis B, Morris M A, Holmes J D and Erts D 2006 High-density arrays of germanium nanowire photoresistors *Adv. Mater.* **18** 1812–6

[6] Colace L, Masini G, Assanto G, Luan H C, Wada K and Kimerling L C 2000 Efficient high-speed near-infrared Ge photodetectors integrated on Si substrates *Appl. Phys. Lett.* **76** 1231–3

[7] Vivien L, Polzer A, Marris-Morini D, Osmond J, Hartmann J M, Crozat P, Cassan E, Kopp C, Zimmermann H and Fédéli J M 2012 Zero-bias 40Gbit/s germanium waveguide photodetector on silicon *Opt. Express* **20** 1096–101

[8] Kim C J, Lee H S, Cho Y J, Kang K and Jo M H 2010 Diameter-dependent internal gain in ohmic Ge nanowire photodetectors *Nano Lett.* **10** 2043–8

[9] Liu J, Cannon D D, Wada K, Ishikawa Y, Jongthammanurak S, Danielson D T, Michel J and Kimerling L C 2005 Tensile strained Ge p-i-n photodetectors on Si platform for C and L band telecommunications *Appl. Phys. Lett.* **87** 011110

[10] Ishikawa Y, Wada K, Liu J, Cannon D D, Luan H C, Michel J and Kimerling L C 2005 Strain-induced enhancement of near-infrared absorption in Ge epitaxial layers grown on Si substrate *J. Appl. Phys.* **98** 013501

[11] Guilloy K, Pauc N, Gassenq A, Gentile P, Tardif S, Rieutord F and Calvo V 2015 Tensile strained germanium nanowires measured by photocurrent spectroscopy and X-ray microdiffraction *Nano Lett.* **15** 2429–33

[12] Vivien L, Rouvière M, Fédéli J-M, Marris-Morini D, Damlencourt J F, Mangeney J, Crozat P, El Melhaoui L, Cassan E, Le Roux X, Pascal D and Laval S 2007 High speed and high responsivity germanium photodetector integrated in a Silicon-On-Insulator microwaveguide *Opt. Express* **15** 9843–8

[13] Vivien L, Osmond J, Fédéli J-M, Marris-Morini D, Crozat P, Damlencourt J-F, Cassan E, Lecunff Y and Laval S 2009 42 GHz pin Germanium photodetector integrated in a silicon-on-insulator waveguide *Opt. Express* **17** 6252–7

[14] Feng D, Liao S, Dong P, Feng N N, Liang H, Zheng D, Kung C C, Fong J, Shafiiha R, Cunningham J, Krishnamoorthy A V. and Asghari M 2009 High-speed Ge photodetector

monolithically integrated with large cross-section silicon-on-insulator waveguide *Appl. Phys. Lett.* **95** 261105

[15] Vivien L, Marris-Morini D, F´d´li J M, Rouvìre M, Damlencourt J F, El Melhaoui L, Le Roux X, Crozat P, Mangeney J, Cassan E and Laval S 2008 Metal-semiconductor-metal Ge photodetectors integrated in silicon waveguides *Appl. Phys. Lett.* **92** 151114

[16] Greil J, Lugstein A, Zeiner C, Strasser G and Bertagnolli E 2012 Tuning the electro-optical properties of germanium nanowires by tensile strain *Nano Lett.* **12** 6230–4

[17] Yan C, Singh N, Cai H, Gan C L and Lee P S 2010 Network-enhanced photoresponse time of Ge nanowire photodetectors *ACS Appl. Mater. Interfaces* **2** 1794–7

[18] Chaisakul P, Marris-Morini D, Isella G, Chrastina D, Le Roux X, Edmond S, Cassan E, Coudevylle J R and Vivien L 2011 Ge/SiGe multiple quantum well photodiode with 30 GHz bandwidth *Appl. Phys. Lett.* **98** 10–3

[19] Nam J H, Alkis S, Nam D, Afshinmanesh F, Shim J, Park J H, Brongersma M, Okyay A K, Kamins T I and Saraswat K 2015 Lateral overgrowth of germanium for monolithic integration of germanium-on-insulator on silicon *J. Cryst. Growth* **416** 21–7

[20] Nam J H, Afshinmanesh F, Nam D, Jung W S, Kamins T I, Brongersma M L and Saraswat K C 2015 Monolithic integration of germanium-on-insulator p-i-n photodetector on silicon *Opt. Express* **23** 15816

[21] Morse M, Dosunmu O, Sarid G and Chetrit Y 2006 Performance of Ge-on-Si p-i-n photodetectors for standard receiver modules *IEEE Photonics Technol. Lett.* **18** 2442–4

[22] Ahn D, Hong C Y, Liu J, Giziewicz W, Beals M, Kimerling L C, Michel J, Chen J and Kärtner F X 2007 High performance, waveguide integrated Ge photodetectors *Opt. Express* **15** 3916–21

[23] Yakimov A I, Dvurechenskii A V, Nikiforov A I and Proskuryakov Y Y 2001 Interlevel Ge/Si quantum dot infrared photodetector *J. Appl. Phys.* **89** 5676–81

[24] Assefa S, Xia F, Bedell S W, Zhang Y, Topuria T, Rice P M and Vlasov Y A 2010 CMOS-integrated high-speed MSM germanium waveguide photodetector *Opt. Express* **18** 4986–99

[25] Chaisakul P, Marris-Morini D, Isella G, Chrastina D, Rouifed M S, Le Roux X, Edmond S, Cassan E, Coudevylle J R and Vivien L 2011 10-Gb/s Ge/SiGe multiple quantum-well waveguide photodetector *IEEE Photonics Technol. Lett.* **23** 1430–2

[26] Wang J and Lee S 2011 Ge-photodetectors for Si-based optoelectronic integration *Sensors* **11** 696–718

[27] Masini G, Colace L, Assanto G, Luan H C and Kimerling L C 2001 High-performance p-i-n Ge on Si photodetectors for the near infrared: From model to demonstration *IEEE Trans. Electron Devices* **48** 1092–6

[28] Roth J E, Fidaner O, Schaevitz R K, Kuo Y-H, Kamins T I, Harris J S and Miller D A 2007 Optical modulator on silicon employing germanium quantum wells *Opt. Express* **15** 5851–9

[29] Liu J, Pan D, Jongthammanurak S, Wada K, Kimerling L C and Michel J 2007 Design of monolithically integrated GeSi electro-absorption modulators and photodetectors on a SOI platform *Opt. Express* **15** 623–8

[30] Feng N-N, Feng D, Liao S, Wang X, Dong P, Liang H, Kung C-C, Qian W, Fong J, Shafiiha R, Luo Y, Cunningham J, Krishnamoorthy A V and Asghari M 2011 30GHz Ge electro-absorption modulator integrated with 3μm silicon-on-insulator waveguide *Opt. Express* **19** 7062–7

[31] Kuo Y, Member S, Lee Y K, Ge Y, Ren S, Roth J E, Kamins T I, Miller D A B and Harris J S 2006 Quantum-confined Stark effect in Ge/SiGe quantum wells on Si for optical modulators *IEEE J. Quantum Electron.* **12** 1503–13

[32] Roth J E, Fidaner O, Edwards E H, Schaevitz R K, Kuo Y-H, Helman N C, Kamins T I, Harris J S and Miller D A B 2008 C-band side-entry Ge quantum-well electroabsorption modulator on SOI operating at 1 V swing *Electron. Lett.* **44** 49

[33] Chaisakul P, Marris-Morini D, Rouifed M-S, Isella G, Chrastina D, Frigerio J, Le Roux X, Edmond S, Coudevylle J-R and Vivien L 2012 23 GHz Ge/SiGe multiple quantum well electro-absorption modulator *Opt. Express* **20** 3219–24

[34] Rouifed M S, Marris-Morini D, Chaisakul P, Frigerio J, Isella G, Chrastina D, Edmond S, Le Roux X, Coudevylle J R, Bouville D and Vivien L 2014 Advances toward Ge/SiGe quantum-well waveguide modulators at 1.3μm *IEEE J. Sel. Top. Quantum Electron.* **20** 49–50

[35] Lever L, Hu Y, Myronov M, Liu X, Owens N, Gardes F Y, Marko I P, Sweeney S J, Ikonić Z, Leadley D R, Reed G T and Kelsall R W 2011 Modulation of the absorption coefficient at 1.3μm in Ge/SiGe multiple quantum well heterostructures on silicon *Opt. Lett.* **36** 4158–60

[36] Stillman G E, Robbins V M and Tabatabaie N 1984 II-V compound semiconductor devices: Optical detectors *IEEE Trans. Electron Devices* **ED-31** 1643–55

[37] Colace L, Masini G, Cencelli V, DeNotaristefani F and Assanto G 2007 A near-infrared digital camera in polycrystalline germanium integrated on silicon *IEEE J. Quantum Electron.* **43** 311–5

[38] Sukhdeo D S, Nam D, Kang J-H, Brongersma M L and Saraswat K C 2014 Direct bandgap germanium-on-silicon inferred from 5.7% ⟨100⟩ uniaxial tensile strain *Photonics Res*. **2** A8–13

[39] El Kurdi M, Fishman G, Sauvage Ś and Boucaud P 2010 Band structure and optical gain of tensile-strained germanium based on a 30 band k·p formalism *J. Appl. Phys*. **107** 013710

[40] Koerner R, Oehme M, Gollhofer M, Schmid M, Kostecki K, Bechler S, Widmann D, Kasper E and Schulze J 2015 Electrically pumped lasing from Ge Fabry-Perot resonators on Si *Opt. Express* **23** 14815–22

[41] Liu J, Sun X, Camacho-Aguilera R, Kimerling L C and Michel J 2010 Ge-on-Si laser operating at room temperature *Opt. Lett*. **35** 679–81

[42] Camacho-Aguilera R E, Cai Y, Patel N, Bessette J T, Romagnoli M, Kimerling L C and Michel J 2012 An electrically pumped germanium laser *Opt. Express* **20** 11316–20

[43] Zhang F, Crespi V H and Zhang P 2009 Prediction that uniaxial tension along <111> produces a direct band gap in germanium *Phys. Rev. Lett*. **102** 1–4

[44] Lim P H, Park S, Ishikawa Y and Wada K 2009 Enhanced direct bandgap emission in germanium by micromechanical strain engineering *Opt. Express* **17** 16358–65

[45] Wirths S, Geiger R, Von Den Driesch N, Mussler G, Stoica T, Mantl S, Ikonic Z, Luysberg M, Chiussi S, Hartmann J M, Sigg H, Faist J, Buca D and Grützmacher D 2015 Lasing in direct-bandgap GeSn alloy grown on Si *Nat. Photonics* **9** 88–92

[46] Fischetti M V and Laux S E 1996 Band structure, deformation potentials, and carrier mobility in strained Si Ge, and SiGe alloys *J. Appl. Phys*. **80** 2234–52

[47] Corp M M and Strengths H 1972 Review: The theoretical strength of solids *J. Mater. Sci.* **7** 239–54

[48] Claeys C and Simoen E 2011 *Germaniun-based technologies: From materials to devices*

[49] Ngo L T, Almécija D, Sader J E, Daly B, Petkov N, Holmes J D, Erts D and Boland J J 2006 Ultimate-strength germanium nanowires *Nano Lett.* **6** 2964–8

[50] Hoffmann S, Utke I, Moser B, Michler J, Christiansen S H, Schmidt V, Senz S, Werner P, Gŏsele U and Ballif C 2006 Measurement of the bending strength of vapor-liquid-solid grown silicon nanowires *Nano Lett.* **6** 622–5

[51] Davidson F M, Lee D C, Fanfair D D and Korgel B A 2007 Lamellar twinning in semiconductor nanowires *J. Phys. Chem. C* **111** 2929–35

[52] Yan R, Gargas D and Yang P 2009 Nanowire photonics *Nat. Photonics* **3** 569–76

[53] Zhu T and Li J 2010 Ultra-strength materials *Prog. Mater. Sci.* **55** 710–57

[54] Smith D A, Holmberg V C and Korgel B A 2010 Flexible germanium nanowires: Ideal strength, room temperature plasticity, and bendable semiconductor fabric *ACS Nano* **4** 2356–62

[55] Roundy D and Cohen M L 2001 Ideal strength of diamond, Si, and Ge *Phys. Rev. B - Condens. Matter Mater. Phys.* **64** 212103

[56] Van De Walle C G 1989 Band lineups and deformation potentials in the model-solid theory *Phys. Rev. B* **39** 1871–83

[57] Geiger R, Zabel T and Sigg H 2015 Group IV direct band gap photonics: Methods, challenges, and opportunities *Front. Mater.* **2** 52

[58] Boucaud P, El Kurdi M, Ghrib A, Prost M, de Kersauson M, Sauvage S, Aniel F, Checoury X, Beaudoin G, Largeau L, Sagnes I, Ndong G, Chaigneau M and Ossikovski R 2013 Recent advances in germanium emission *Photonics Res*. **1** 102–9

[59] Cheng T H, Peng K L, Ko C Y, Chen C Y, Lan H S, Wu Y R, Liu C W and Tseng H H 2010 Strain-enhanced photoluminescence from Ge direct transition *Appl. Phys. Lett*. **96** 94–7

[60] Dutt B, Sukhdeo D S, Nam D, Vulovic B M, Yuan Z and Saraswat K C 2012 Roadmap to an efficient germanium-on-silicon laser: Strain vs. n-type doping *IEEE Photonics J*. **4** 2002–9

[61] Nam D, Sukhdeo D S, Gupta S, Kang J H, Brongersma M L and Saraswat K C 2014 Study of Carrier Statistics in Uniaxially Strained Ge for a Low-Threshold Ge Laser *IEEE J. Sel. Top. Quantum Electron*. **20** 16–22

[62] Sukhdeo D S, Kim Y, Gupta S, Saraswat K C, Dutt B R and Nam D 2016 Anomalous threshold reduction from <100> uniaxial strain for a low-threshold Ge laser *Opt. Commun*. **379** 32–5

[63] Nam D 2013 Strained germanium technology for on-chip optical interconnects *STANFORD PhD Thesis* 113

[64] Sukhdeo D S, Gupta S, Saraswat K C, Dutt B and Nam D 2016 Impact of minority carrier lifetime on the performance of strained germanium light sources *Opt. Commun*. **364** 233–7

[65] Nam D, Kang J-H, Brongersma M L and Saraswat K C 2014 Observation of improved minority carrier lifetimes in high-quality Ge-on-insulator using time-resolved photoluminescence *Opt. Lett*. **39** 6205–8

[66] Sukhdeo D S, Gupta S, Saraswat K C, Dutt B R and Nam D 2016 Ultimate limits of biaxial tensile strain and n-type doping for realizing an efficient low-threshold Ge laser *Jpn. J. Appl. Phys.* **55** 024301

[67] Lee A J, Kim M, Lena C and Chelikowsky J R 2012 Mechanical and electronic properties of strained Ge nanowires using ab initio real-space pseudopotentials *Phys. Rev. B - Condens. Matter Mater. Phys.* **86** 1–6

[68] Haugerud B M, Bosworth L A and Belford R E 2003 Mechanically induced strain enhancement of metal-oxide-semiconductor field effect transistors *J. Appl. Phys.* **94** 4102–7

[69] Huang S and Yang L 2011 Strain engineering of band offsets in Si/Ge core-shell nanowires *Appl. Phys. Lett.* **98** 2009–12

[70] Sukhdeo D S, Nam D, Kang J-H, Brongersma M L and Saraswat K C 2015 Bandgap-customizable germanium using lithographically determined biaxial tensile strain for silicon-compatible optoelectronics *Opt. Express* **23** 16740

[71] de Kersauson M, Kurdi M El, David S, Checoury X, Fishman G, Sauvage S, Jakomin R, Beaudoin G, Sagnes I and Boucaud P 2011 Optical gain in single tensile-strained germanium photonic wire *Opt. Express* **19** 17925–34

[72] Keplinger M, Grifone R, Greil J, Kriegner D, Persson J, Lugstein A, Schülli T and Stangl J 2016 Strain distribution in single, suspended germanium nanowires studied using nanofocused x-rays *Nanotechnology* **27** 55705

[73] Dupré L, Buttard D, Gentile P, Benoit à la Guillaume Q, Gorisse T and Renevier H 2014 Strain control in germanium nanowires: The use of a silicon nitride shell *Phys. Status Solidi - Rapid Res. Lett.* **8** 317–20

[74] Audoit G, Mhuircheartaigh É N, Lipson S M, Morris M A, Blau W J and Holmes J D 2005 Strain induced photoluminescence from silicon and germanium nanowire arrays *J. Mater. Chem.* **15** 4809–15

[75] Jung D, Faucher J, Mukherjee S, Akey A, Ironside D J, Cabral M, Sang X, Lebeau J, Bank S R, Buonassisi T, Moutanabbir O and Lee M L 2017 Highly tensile-strained Ge/InAlAs nanocomposites *Nat. Commun.* **8** 1–7

[76] Süess M J, Geiger R, Minamisawa R A, Schiefler G, Frigerio J, Chrastina D, Isella G, Spolenak R, Faist J and Sigg H 2013 Analysis of enhanced light emission from highly strained germanium microbridges *Nat. Photonics* **7** 466–72

[77] Nam D, Sukhdeo D S, Kang J H, Petykiewicz J, Lee J H, Jung W S, Vučković J, Brongersma M L and Saraswat K C 2013 Strain-induced pseudoheterostructure nanowires confining carriers at room temperature with nanoscale-tunable band profiles *Nano Lett.* **13** 3118–23

[78] Menon M, Srivastava D, Ponomareva I and Chernozatonskii L A 2004 Nanomechanics of silicon nanowires *Phys. Rev. B - Condens. Matter Mater. Phys.* **70** 125313

[79] Kuroyanagi R, Nguyen L M, Tsuchizawa T, Ishikawa Y, Yamada K and Wada K 2013 Local bandgap control of germanium by silicon nitride stressor *Opt. Express* **21** 18553–7

[80] Jain J R, Hryciw A, Baer T M, Miller D A B, Brongersma M L and Howe R T 2012 A micromachining-based technology for enhancing germanium light emission via tensile strain *Nat. Photonics* **6** 398–405

[81] Ghrib A, Kurdi M El, Kersauson M De, Prost M, Sauvage S and Checoury X 2016 Tensile-strained germanium microdisks *Appl. Phys. Lett.* **102** 221112

[82] Capellini G, Reich C, Guha S, Yamamoto Y, Lisker M, Virgilio M, Ghrib A, Kurdi M El, Boucaud P, Tillack B and Schroeder T 2014 Tensile Ge microstructures for lasing fabricated by means of a silicon complementary metal-oxide-semiconductor process *Opt. Express* **22** 102–9

[83] Nam D, Sukhdeo D, Roy A, Balram K, Cheng S-L, Huang K C-Y, Yuan Z, Brongersma M, Nishi Y, Miller D and Saraswat K 2011 Strained germanium thin film membrane on silicon substrate for optoelectronics *Opt. Express* **19** 25866–72

[84] Nam D, Sukhdeo D, Cheng S L, Roy A, Chih-Yao Huang K, Brongersma M, Nishi Y and Saraswat K 2012 Electroluminescence from strained germanium membranes and implications for an efficient Si-compatible laser *Appl. Phys. Lett.* **100** 1–5

[85] Oda K, Okumura T, Tani K, Saito S I and Ido T 2014 Improvement of photoluminescence from Ge layer with patterned Si_3N_4 stressors *Thin Solid Films* **557** 355–62

[86] Sukhdeo D S, Petykiewicz J, Gupta S, Kim D, Woo S, Kim Y, Vučković J, Saraswat K C and Nam D 2015 Ge microdisk with lithographically-tunable strain using CMOS-compatible process *Opt. Express* **23** 33249

[87] Minamisawa R A, Süess M J, Spolenak R, Faist J, David C, Gobrecht J, Bourdelle K K and Sigg H 2012 Top-down fabricated silicon nanowires under tensile elastic strain up to 4.5% *Nat. Commun.* **3** 1096

[88] Ishikawa Y, Wada K, Cannon D D, Liu J, Luan H C and Kimerling L C 2003 Strain-induced band gap shrinkage in Ge grown on Si substrate *Appl. Phys. Lett.* **82** 2044–6

[89] Hu S, Kawamura Y, Huang K C Y, Li Y, Marshall A F, Itoh K M, Brongersma M L and McIntyre P C 2012 Thermal stability and surface passivation of Ge nanowires coated by epitaxial SiGe shells *Nano Lett*. **12** 1385–91

[90] Goldthorpe I A, Marshall A F and McIntyre P C 2009 Inhibiting strain-induced surface roughening: Dislocation-free Ge/Si and Ge/SiGe core-shell nanowires *Nano Lett*. **9** 3715–9

[91] Goldthorpe I A, Marshall A F and Mcintyre P C 2008 Synthesis and strain relaxation of Ge-core/Si-shell nanowire arrays *Nano Lett*. **8** 4081–6

[92] Bao S, Kim D, Onwukaeme C, Gupta S, Saraswat K, Lee K H, Kim Y, Min D, Jung Y, Qiu H, Wang H, Fitzgerald E A, Tan C S and Nam D 2017 Low-threshold optically pumped lasing in highly strained germanium nanowires *Nat. Commun*. **8** 1–7

[93] Petykiewicz J, Nam D, Sukhdeo D S, Gupta S, Buckley S, Piggott A Y, Vučković J and Saraswat K C 2016 Direct bandgap light emission from strained germanium nanowires coupled with high-Q nanophotonic cavities *Nano Lett*. **16** 2168–73

[94] Gupta S, Nam D, Vuckovic J and Saraswat K 2018 Room temperature lasing unraveled by a strong resonance between gain and parasitic absorption in uniaxially strained germanium *Phys. Rev. B* **97** 1–9

[95] Koerner R, Schwaiz D, Fischer I A, Augel L, Bechler S, Haenel L, Kern M, Oehme M, Rolseth E, Schwartz B, Weisshaupt D, Zhang W and Schulze J 2017 The Zener-Emitter: A novel superluminescent Ge optical waveguide-amplifier with 4.7 dB gain at 92 mA based on free-carrier modulation by direct Zener tunneling monolithically integrated on Si *Technical Digest - International Electron Devices Meeting, IEDM* p 22.5.1-22.5.4

[96] Ellis B, Mayer M A, Shambat G, Sarmiento T, Harris J, Haller E E and Vučković J 2011 Ultralow-threshold electrically pumped quantum-dot photonic-crystal nanocavity laser *Nat. Photonics* **5** 297–300

[97] Jeong K Y, No Y S, Hwang Y, Kim K S, Seo M K, Park H G and Lee Y H 2013 Electrically driven nanobeam laser *Nat. Commun.* **4** 2822

[98] Thareja G, Chopra S, Adams B, Kim Y, Moffatt S, Saraswat K and Nishi Y 2011 High n-type antimony dopant activation in germanium using laser annealing for n+/p junction diode *IEEE Electron Device Lett.* **32** 838–40

[99] Chui C O, Gopalakrishnan K, Griffin P B, Plummer J D and Saraswat K C 2003 Activation and diffusion studies of ion-implanted p and n dopants in germanium *Appl. Phys. Lett.* **83** 3275–7

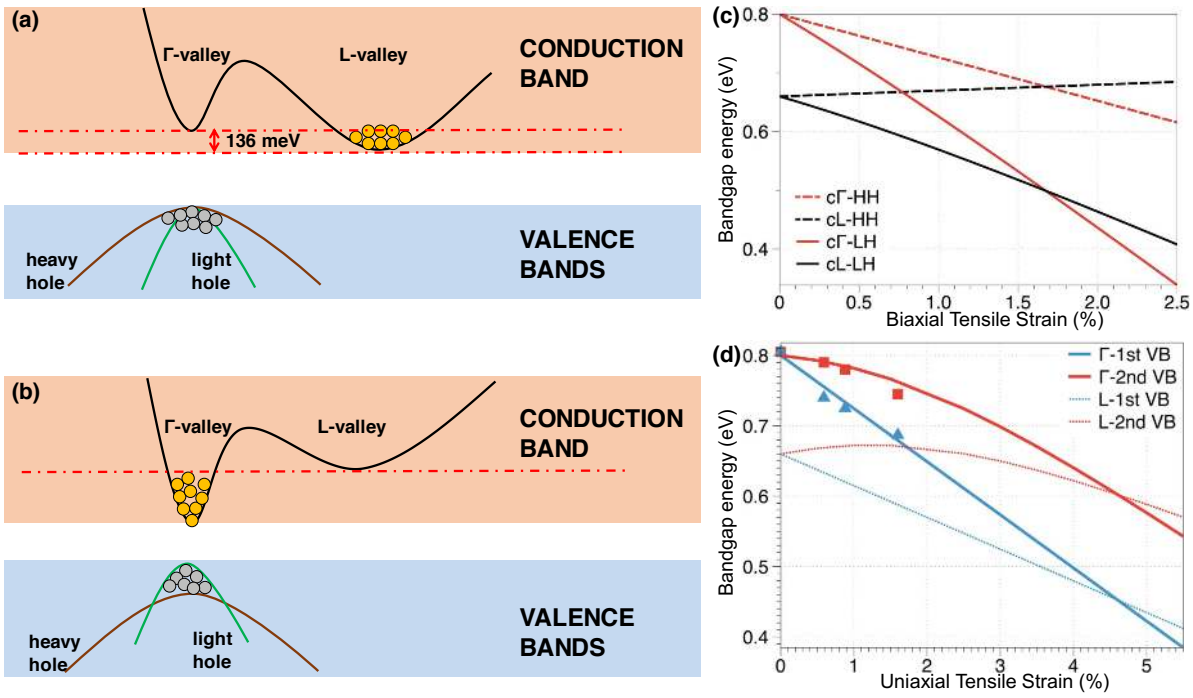

Figure 1. Bandstructures and bandgap energies of strained and unstrained Ge. (a) Schematic of an unstrained Ge bandstructure. Electrons prefer to occupy the lowest conduction band (*i.e.*, L-valley). (b) Schematic of a strained Ge bandstructure. In highly tensile strained Ge, the direct bandgap shrinks greatly and the fraction of electrons in the Γ-valley increases. (c,d) Calculated bandgap energies in Ge as a function of (c) biaxial and (d) uniaxial tensile strains. Reproduced with permission [63]. Copyright 2013, Stanford University.

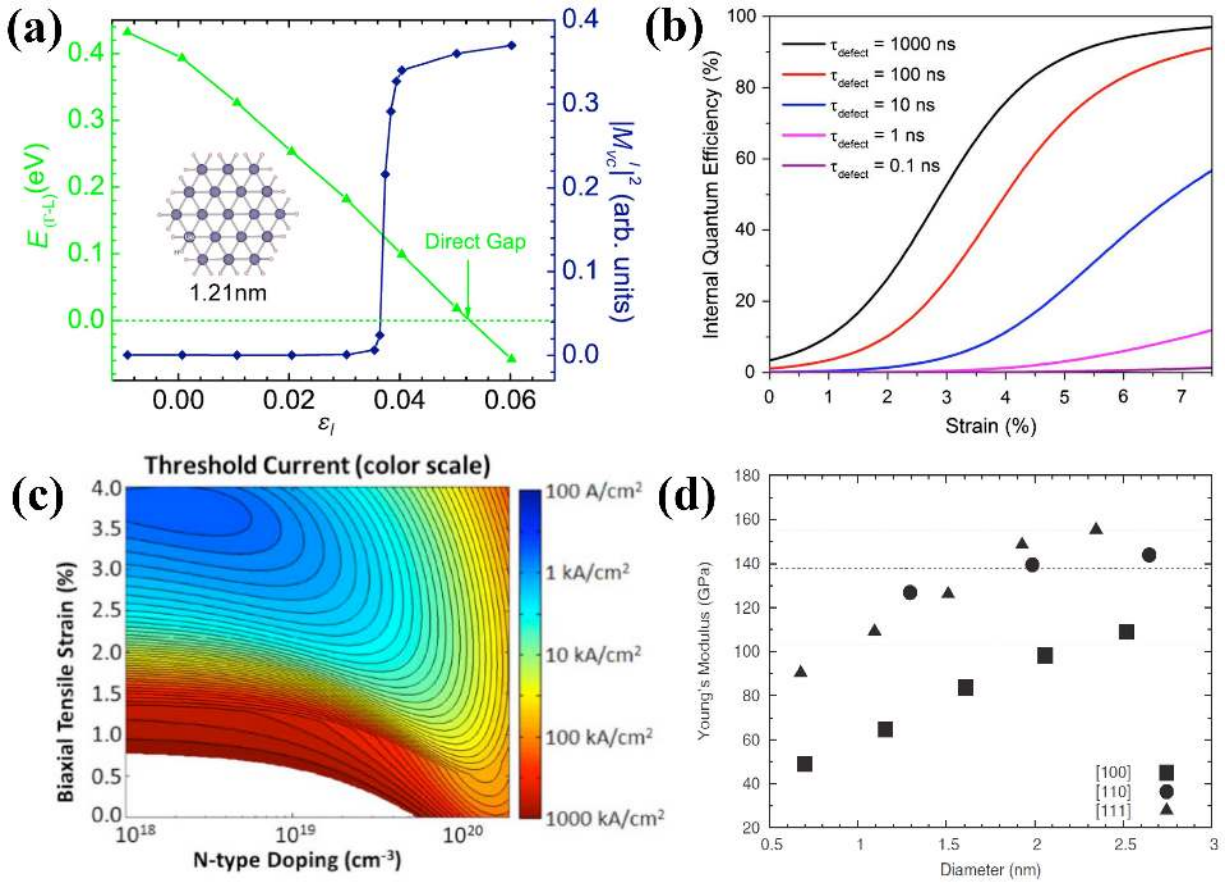

Figure 2. Effects of strain on Ge's optical and mechanical properties. (a) $E_{(\Gamma\text{-}L)}$ and M^{l}_{vc} as a function of strain for a Ge NW with a diameter of 1.21 nm. Reproduced with permission [43]. Copyright 2009, American Physical Society. (b) Theoretically calculated IQE of a Ge LED as a function of uniaxial tensile strain for various defect-assisted recombination lifetimes. Reproduced with permission [38]. Copyright 2014, Chinese Laser Press. (c) Calculated threshold current density as a function of strain and n-type doping with an assumption of a lossless cavity. Reproduced with permission [66]. Copyright 2016, The Japan Society of Applied Physics. (d) Calculated Young's modulus as a function of Ge NW diameter for different growth directions. The dashed lines represent the calculated values for bulk Ge. Reproduced with permission [67]. Copyright 2012, American Physical Society.

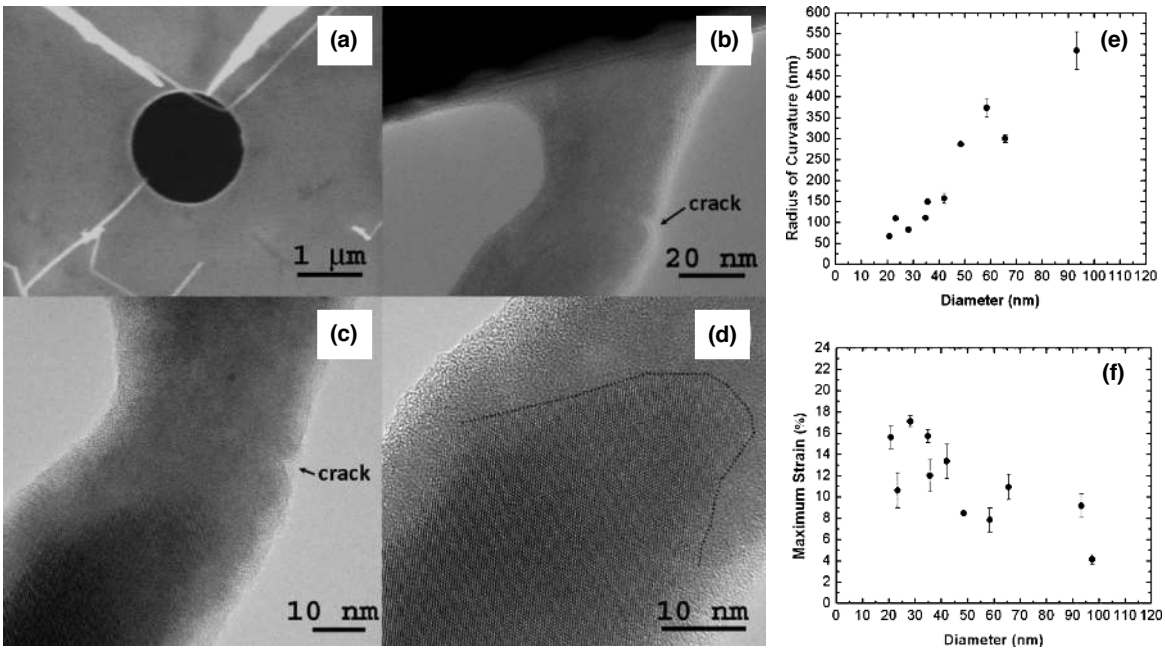

Figure 3. Mechanical bending of Ge NWs. (a) Scanning electron microscope (SEM) image of a bent Ge NW. (b,c) TEM images of the highest strain region with the appearance of crack formation. (d) TEM image showing the single-crystal and amorphous phases in the strain area. (e) Measured maximum radius of curvature as a function of Ge NW diameter. (f) Measured maximum strain as a function of Ge NW diameter. Reproduced with permission [54]. Copyright 2010, American Chemical Society.

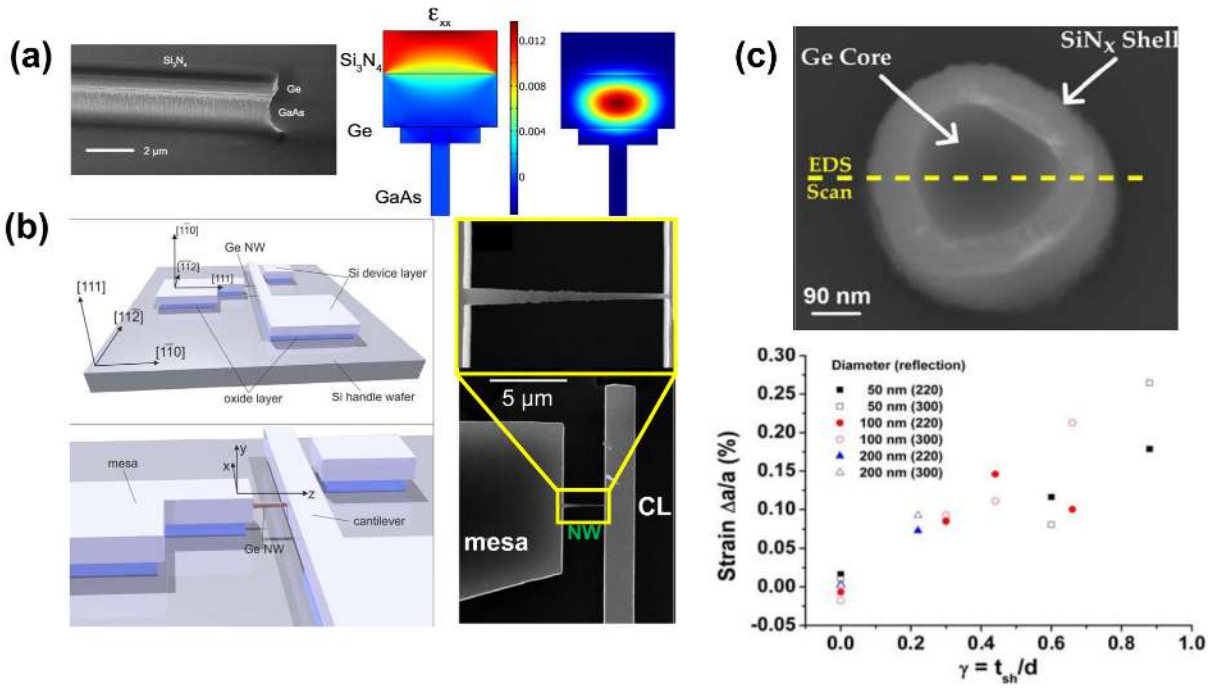

Figure 4. Stressor-induced tensile strain in Ge NWs based on microfabrication and epitaxy technologies. (a) Tensile strained Ge NW waveguide structure. Distributions of strain and transverse magnetic (TM) optical mode in the NW are calculated. Reproduced with permission [71]. Copyright 2011, Optical Society of America. (b) Schematic views and SEM images showing that the Ge NW can be highly strained by using a pre-stressed cantilever. Reproduced with permission [72]. Copyright 2016, Institute of Physics. (c) SEM image of the cross-sectional view of a Ge-SiN_x core-shell nanostructure. The strain obtained in Ge NW is studied as a function of the core-shell structural parameter γ which is the ratio of shell thickness to NW diameter. Reproduced with permission [73]. Copyright 2014, John Wiley & Sons, Inc.

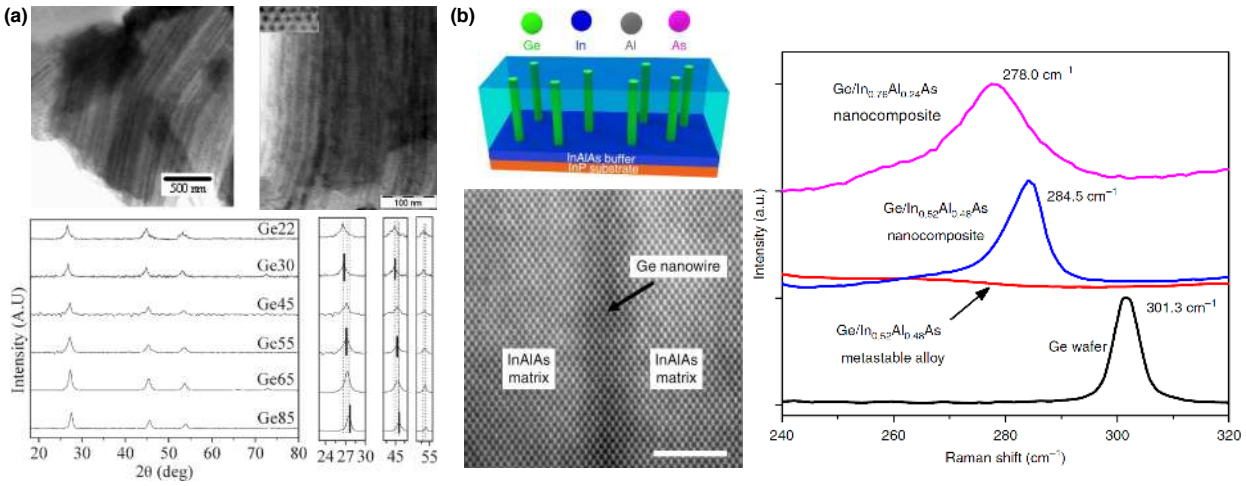

Figure 5. Tensile-strained Ge NW nanocomposites. (a) TEM images of two nanocomposite samples with mean Ge NW diameters of 65 Å (left) and 55 Å (right). PXRD patterns for the Ge/SiO_2 nanocomposites with different pore diameters after background subtraction. Reproduced with permission [74]. Copyright 2005, Royal Society of Chemistry. (b) Highly tensile-strained Ge/InAlAs nanocomposites. Raman spectra of bulk Ge, Ge/InAlAs metastable alloy, and two kinds of Ge/InAlAs nanocomposites with different contents are measured. Reproduced with permission [75]. Copyright 2017, Nature Publishing Group.

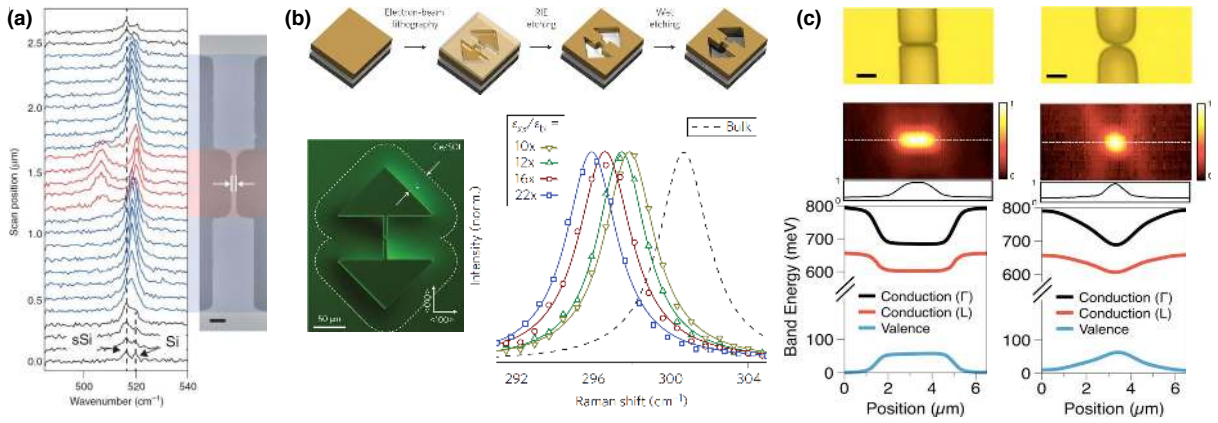

Figure 6. Geometrical strain amplification method. (a) A dumbbell-like strained Si NW bridge. Raman spectra at different locations show highly strained Si NWs as shown in red spectra. Reproduced with permission [87]. Copyright 2012, Nature Publishing Group. (b) A highly strained Ge bridge structure on a Ge/SOI platform. Normalized Raman spectra for different enhancement factors (EFs) are measured. Reproduced with permission [76]. Copyright 2013, Nature Publishing Group. (c) Strained Ge pseudo-heterostructure NWs. Optical micrographs and 2D PL maps of an s-DH and an s-GDH show enhanced and spatially confined light emissions from the strain-induced potential wells. Band diagrams are calculated within the active regions of the s-DH and s-GDH. Reproduced with permission [77]. Copyright 2013, American Chemical Society.

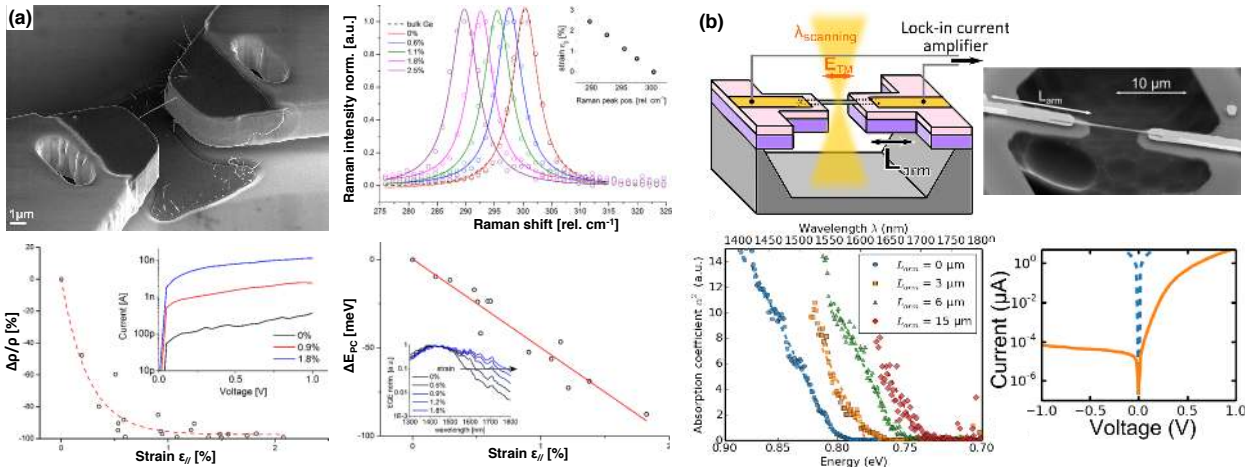

Figure 7. Strained Ge NW photodetectors. (a) A suspended Ge NW bridging two Si pads along the <111> direction. Normalized Raman spectra, relative change in resistivity, and photocurrent spectra of strained Ge NWs are studied with different tensile strain values. Reproduced with permission [16]. Copyright 2012, American Chemical Society. (b) A suspended Ge NW anchored between two Si_3N_4 pulling arms. Photocurrent spectra of stressed Ge NWs are measured with different pulling arm lengths. The electrical properties of the NW p-i-n junction before and after etching are investigated based on their I-V characteristics (on a logarithmic scale). Reproduced with permission [11]. Copyright 2015, American Chemical Society.

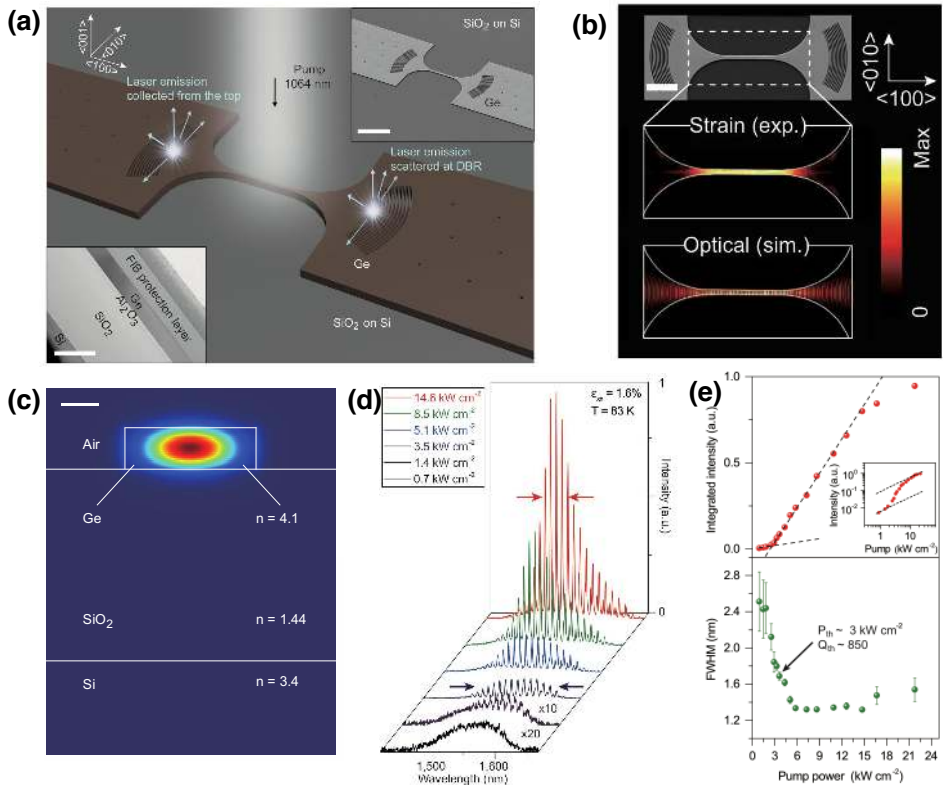

Figure 8. Strained Ge NW lasers. (a) Schematic view of a Ge NW laser containing a strained NW gain medium surrounded by a pair of DBRs on the stressing pads. (b) Experimental strain mapping and simulated optical field distribution. (c) Simulated TE mode distribution. (d) Pump-dependent PL spectra of a 1.6%-tensile strained Ge NW laser. (e) Integrated PL intensity and linewidth evolution versus optical pump power. Reproduced with permission [92]. Copyright 2017, Nature Publishing Group.